Distilling one, two and entangled pairs of photons from a quantum dot with cavity QED effects and spectral filtering

New Journal of Physics

Distilling one, two and entangled pairs of photons from a quantum dot with cavity QED effects and spectral filtering

Elena del Valle

Physik Department, Technische Universität München, James-Franck-Strasse, D-85748 Garching, Germany
E-mail: elena.delvalle.reboul@gmail.com

Abstract. A quantum dot can be used as a source of one- and two-photon states and of polarization entangled photon pairs. The emission of such states is investigated here from the point of view of frequency-resolved two-photon correlations. These follow from a spectral filtering of the dot emission, which can be achieved either by using a cavity or by placing a number of interference filters before the detectors. A combination of these various options is used to iteratively refine the emission in a 'distillation' process and arrive at highly correlated states with a high purity. The so-called 'leapfrog processes', where the system undergoes a direct transition from the biexciton state to the ground state by direct emission of two photons, are shown to be central to the quantum features of such sources. Optimum configurations are singled out in a global theoretical picture that unifies the various regimes of operation.

IOP Institute of Physics ⦶ DEUTSCHE PHYSIKALISCHE GESELLSCHAFT

Contents

1. Introduction

Quantum dots have proven in recent years to be an excellent platform for single-photon sources [1–3], spin manipulation and coherent control at the exciton [4–8] or biexciton level [9–14] or for entangled photon-pair generation [15–17]. The achievement of strong coupling between a single quantum dot and a cavity mode [18–20] kindled these possibilities even further by increasing their efficiency and output-collectability [21, 22] to the point of reaching new regimes such as microlasing [23] or two-photon emission [24]. The cavity mode can also serve as a coupler between two distant dots [25, 26]. Cavity QED effects are thus a powerful resource to exploit the quantum features of a quantum dot [27–30].

There is an alternative way to control, engineer and purify the emission of a quantum emitter which relies on extrinsic components at the macroscopic level, in contrast with the intrinsic approach at the microscopic level that supplements the quantum dot with a built-in microcavity. Namely, one can use spectral filtering. This approach is 'extrinsic' in the sense that the filters are placed between the system that emits the light and the observer who detects it. As such, it belongs more properly to the detection part. The filter can in fact be modelling the finite resolution of a detector that is sensible only within a given frequency window. In this paper, to keep the discussion as simple as possible, we will assume perfect detectors and describe the detection process through spectral filters (this means that the detector has a better resolution than that imparted by the filter in front of it). Each filter is theoretically fully specified by its central frequency of detection and linewidth. We will assume Lorentzian spectral shapes, which correspond to the case of most interference filters. Commonly used spectral filters of this type are the thin-film filters and Fabry–Perot interferometers (in the figures, we will sketch such filters as dichroic bandpass filters, with different colours to imply different frequencies). Since
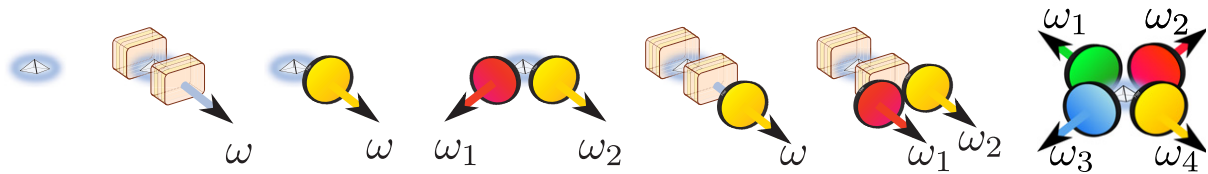
Figure 1. Sketch of the various schemes investigated in this work to study two-photon correlations from the light emitted by a quantum dot (left). The various detection configurations are, from left to right: (i) the direct emission of the dot ($g^{(2)}[\sigma_H]$), (ii) the enhanced and filtered emission of the dot by a cavity mode ($g^{(2)}[a]$); (iii), the filtered emission of the dot ($g_\Gamma^{(2)}[\sigma_H](\omega; \omega)$), (iv) the two-photon spectroscopy of the dot ($g_\Gamma^{(2)}[\sigma_H](\omega_1; \omega_2)$), (v) the filtered emission of the dot-in-a-cavity emission ($g_\Gamma^{(2)}[a](\omega; \omega)$), (vi) the two-photon spectroscopy of the dot-in-a-cavity ($g_\Gamma^{(2)}[a](\omega_1; \omega_2)$) and (vii) the tomographic reconstruction of the density matrix for the polarization-entangled photon pairs, $\theta_\Gamma(\omega_1, \omega_2; \omega_3, \omega_4)$.

they rely on interference effects, they are basically cavities in weak-coupling. This reinforces the main theme of this paper, which is to investigate cavity effects on a quantum emitter. The cavity itself can be, again, intrinsically part of the heterostructure itself, all packaged on-chip, or extrinsically realized by the external filters. Combining these features, such as filtering the emission of a cavity–QED system, we arrive at the notion of 'distillation' where the emitter sees its output increasingly filtered by consecutive sequences to finally deliver a highly correlated quantum state of high purity.

While the idea is general and could be applied to a wealth of quantum emitters, we concentrate here on a single quantum dot, sketched as a little radiating pyramid in figure 1. Theoretically, it will be described as a combination of two two-level systems, representing two excitons of opposite spins. Such a system will be used for the generation of photons one by one or in pairs, with various types of quantum correlations. The four-level system formed by the two possible excitonic states (corresponding to orthogonal polarizations) and the doubly occupied state, the biexciton, is ideal to switch from one type of device to the other by simply selecting and enhancing the emission at different intrinsic resonances [31–33]. Figure 1 gives a summary of the various filtering and detection schemes that will be applied, with the 'naked' dot on the left. Its emission will be considered both from within or without a cavity, with various numbers of filters interceding. We will assume the microcavity both in the weak- and strong-coupling regimes. The latter system has been extensively studied [31–35] and will be revisited here in the light of its spectral filtering [36] and distillation.

The rest of the paper is organized as follows. In section 2, we present the system and its basic properties and we introduce the *two-photon spectrum*, which is the counterpart at the two-photon level of the photoluminescence spectrum at the single-photon one. In section 3, we provide the first application of two-photon distillation, achieved via a cavity mode weakly coupled to the dot transitions or through spectral filtering. In section 4, we compare the cavity filtering in the weak-coupling regime with the enhancement of emission in the strong-coupling regime. In section 4.1, we go one step further in the distillation of the two-photon emission and filter it from the cavity emission as well. In section 5, we consider one of the most popular applications of the biexciton structure, the generation of polarization entangled photon pairs. In section 6, we draw some conclusions.
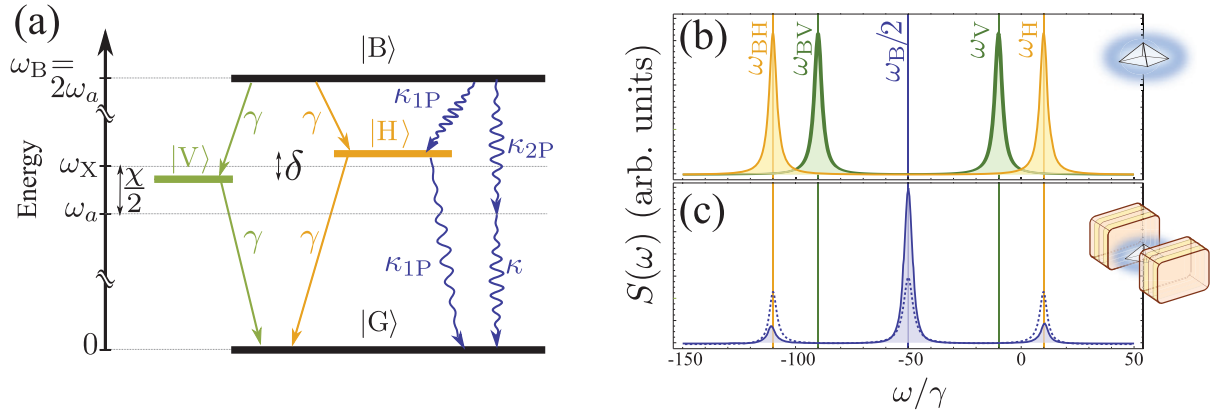
Figure 2. (a) Level scheme of the quantum dot investigated, modelled as a system able to accommodate two excitons $|V\rangle$ and $|H\rangle$ in the linear polarization basis, with an energy splitting δ between them and which, when present jointly, form a biexciton $|B\rangle$ with binding energy χ. The excitons decay radiatively at a rate γ. When placed in a cavity (with linear polarization H), two extra decay channels are opened for the H-polarization: through the one-photon cascade at rate κ_{1P} and the two-photon emission at rate κ_{2P}. In the sketch, the cavity is placed at the two-photon resonance $\omega_a = \omega_B/2$. (b) PL spectra from the quantum dot system in H-polarization (orange) consisting of two peaks at ω_{BH} and ω_H, and in V-polarization (green) consisting of two peaks at ω_{BV} and ω_V. (c) PL spectrum when the dot is placed inside a cavity, both for the case of strong ($g = \kappa$, solid line) and weak ($g \to 0$, dotted line) coupling. A new peak appears at the centre from the two-photon emission. Parameters: $P = \gamma$, $\chi = 100\gamma$, $\delta = 20\gamma$ and $\kappa = 5\gamma$. We consider $\omega_X \to 0$ as the reference frequency.

2. Analysis of the quantum dot direct emission

2.1. Theoretical model and standard characterization

The system under analysis consists of a quantum dot that can host up to two excitons with opposite spins. The corresponding orthonormal basis of linear polarizations, horizontal (H) and vertical (V), reads $\{|G\rangle, |H\rangle, |V\rangle, |B\rangle\}$, where G stands for the ground state, H and V for the single exciton states and B for the biexciton or doubly occupied state. The four-level scheme that they form is depicted in figure 2(a). The Hamiltonian of the system reads ($\hbar = 1$)

$$H_{\text{dot}} = \left(\omega_X + \frac{\delta}{2}\right)|H\rangle\langle H| + \left(\omega_X - \frac{\delta}{2}\right)|V\rangle\langle V| + \omega_B|B\rangle\langle B|, \tag{1}$$

where we allow the excitonic states to be split by a small energy δ, as is typically the case experimentally, through the so-called *fine structure splitting* [24]. The biexciton at $\omega_B = 2\omega_X - \chi$ is far detuned from twice the exciton thanks to the binding energy, χ, typically the largest parameter in the system. We include the dot losses, at a rate γ, and an incoherent continuous excitation (off-resonant driving of the wetting layer), at a rate P, in both polarizations $x =$H, V,

in a master equation

$$\partial_t \rho = i[\rho, H_{\mathrm{dot}}] + \sum_{x=\mathrm{H,V}} \left[\frac{\gamma}{2}\left(\mathcal{L}_{|\mathrm{G}\rangle\langle x|} + \mathcal{L}_{|x\rangle\langle\mathrm{B}|}\right) + \frac{P}{2}\left(\mathcal{L}_{|x\rangle\langle\mathrm{G}|} + \mathcal{L}_{|\mathrm{B}\rangle\langle x|}\right)\right](\rho), \qquad (2)$$

where $\mathcal{L}_c(\rho) = 2c\rho c^\dagger - c^\dagger c\rho - \rho c^\dagger c$ is in the Lindblad form. In this work, we are interested in the steady state of the system resulting from the interplay between the incoherent continuous pump and decay of the quantum dot levels.

We assume in what follows an experimentally relevant situation, $\chi = 100\gamma$, $\delta = 20\gamma$, and study the steady state under $P = \gamma$, in which case all levels are equally populated (the populations read $\rho_\mathrm{G} = \gamma^2/(P+\gamma)^2$, $\rho_\mathrm{H} = \rho_\mathrm{V} = P\gamma/(P+\gamma)^2$ and $\rho_\mathrm{B} = P^2/(P+\gamma)^2$). The photoluminescence spectra of the system, $S(\omega)$, are shown in figure 2(b) for the H- and V-polarized emission with orange and green lines, respectively. The four peaks are well separated thanks to the binding energy and fine structure splitting, corresponding to the four transitions depicted in panel (a) with the same colour code

$$\omega_{\mathrm{BH}} = \omega_\mathrm{B} - \omega_\mathrm{H} = \omega_\mathrm{X} - \chi - \delta/2 = -110\gamma, \qquad (3)$$

$$\omega_\mathrm{H} = \omega_\mathrm{X} + \delta/2 = 10\gamma, \qquad (4)$$

$$\omega_{\mathrm{BV}} = \omega_\mathrm{B} - \omega_\mathrm{V} = \omega_\mathrm{X} - \chi + \delta/2 = -90\gamma, \qquad (5)$$

$$\omega_\mathrm{V} = \omega_\mathrm{X} - \delta/2 = -10\gamma \qquad (6)$$

with $\omega_X \to 0$ as the reference and full-width at half-maximum $\gamma_{\mathrm{BH}} = \gamma_{\mathrm{BV}} = 3\gamma + P$, $\gamma_\mathrm{H} = \gamma_\mathrm{V} = 3P + \gamma$. We concentrate on the H-mode emission because it has the largest peak separation and allows for the best filtering but all results apply similarly to the V polarization. The emission structure at the single-photon level is very simple: two Lorentzian peaks are observed corresponding to the upper and lower transitions

$$S[\sigma_\mathrm{H}](\omega) = \frac{1}{\pi}\left[\rho_\mathrm{B}\frac{\gamma_{\mathrm{BH}}/2}{(\gamma_{\mathrm{BH}}/2)^2 + (\omega - \omega_{\mathrm{BH}})^2} + \rho_\mathrm{H}\frac{\gamma_\mathrm{H}/2}{(\gamma_\mathrm{H}/2)^2 + (\omega - \omega_\mathrm{H})^2}\right]. \qquad (7)$$

The second-order coherence function of the H-emission in the steady state (set as the starting time $t = 0$) with a positive delay τ, reads

$$g^{(2)}[\sigma_\mathrm{H}](\tau) = \langle\sigma_\mathrm{H}^+(0)\sigma_\mathrm{H}^+(\tau)\sigma_\mathrm{H}(\tau)\sigma_\mathrm{H}(0)\rangle/\langle\sigma_\mathrm{H}^+\sigma_\mathrm{H}\rangle^2, \qquad (8)$$

where the H-photon destruction operator is defined as

$$\sigma_\mathrm{H} = s_1 + s_2, \quad \text{with} \quad s_1 = |\mathrm{H}\rangle\langle\mathrm{B}| \quad \text{and} \quad s_2 = |\mathrm{G}\rangle\langle\mathrm{H}|. \qquad (9)$$

In equations (7) and (8), we have specified the channel of emission in square brackets, since this will be an important attribute in the rest of the paper. Surprisingly, the quantum dot described with the spin degree of freedom always exhibits uncorrelated statistics in the linear polarization

$$g^{(2)}[\sigma_\mathrm{H}](\tau) = 1. \qquad (10)$$

One recovers the expected antibunching of a two-level system [37] by turning to the intrinsic two-level systems composing the quantum dot, namely, the spin-up and spin-down excitons: $g^{(2)}[\sigma_\uparrow](0) = g^{(2)}[\sigma_\downarrow](0) = 0$. The Pauli exclusion principle that holds for the spin $\sigma_{\uparrow\downarrow}$ breaks in the linear polarization, i.e. while $\sigma_{\uparrow\downarrow}^2 = 0$, one has $\sigma_\mathrm{H}^2 = |\mathrm{G}\rangle\langle\mathrm{B}| \neq 0$. We can find a simple

explanation for this if we write the total correlations in terms of the four contributions (different from zero)

$$\langle \sigma_H^+(0)\sigma_H^+(\tau)\sigma_H(\tau)\sigma_H(0)\rangle = \sum_{i,j=1,2} \langle s_i^+(0)s_j^+(\tau)s_j(\tau)s_i(0)\rangle, \tag{11}$$

which are given by ($\tau \geqslant 0$)

$$g^{(2)}[s_1; s_1](\tau) = (1 - e^{-(\gamma+P)\tau})\left(1 + \frac{\gamma}{P}e^{-(\gamma+P)\tau}\right),$$

$$g^{(2)}[s_2; s_2](\tau) = (1 - e^{-(\gamma+P)\tau})\left(1 + \frac{P}{\gamma}e^{-(\gamma+P)\tau}\right),$$

$$g^{(2)}[s_1; s_2](\tau) = (1 - e^{-(\gamma+P)\tau}) + e^{-(\gamma+P)\tau}\left(2 + \frac{\gamma}{P} + \frac{P}{\gamma}\right),$$

$$g^{(2)}[s_2; s_1](\tau) = (1 - e^{-(\gamma+P)\tau})^2 \tag{12}$$

in their normalized form, $g^{(2)}[s_i; s_j](\tau) = \langle s_i^+(0)s_j^+(\tau)s_j(\tau)s_i(0)\rangle/(\langle s_i^+ s_i\rangle\langle s_j^+ s_j\rangle)$. As shown in figures 3(c) and (d) with pale grey lines, all these functions are antibunched except for $g^{(2)}[s_1; s_2](\tau)$, which corresponds to the natural order in the H-cascaded emission of two photons and is, consequently, bunched. It compensates fully for the other three terms, leading to total correlations of 1 at all τ.

2.2. Two-photon spectrum

Figure 2 provides a clear picture of the physical grounds on which such a system can be used as a quantum emitter, but it lacks even a qualitative picture of how quantum correlations are distributed. Figure 2(b) merely shows where the system emits light but nothing on how correlated is this emission. All these crucial features are revealed in the *two-photon spectrum* $g_\Gamma^{(2)}(\omega_1; \omega_2, \tau)$ [38]. This is the extension of the Glauber second-order coherence function—which quantifies the correlations between photons in their arrival times—to frequency. By specifying both the energy (ω_1 and ω_2) and time of arrival ($t = 0$ and $t = \tau \geqslant 0$) of the photons, one provides an essentially complete description of the system. Γ denotes the linewidth of the frequency window of the filter over which this joint characterization is obtained. The corresponding time resolution is given by its inverse, $1/\Gamma$, in accordance with the Heisenberg uncertainty principle. It is a necessary variable without which nonsensical or trivial results are obtained.

The two-photon spectrum unravels a large class of processes hidden in single-photon spectroscopy and can be expected to become a standard tool to characterize and engineer quantum sources. The computation of such a quantity[1] has remained a challenging task for theorists since the mid-eighties [39–41], until a recent workaround [36] has been found which allows an exact numerical computation. The method consists in coupling very weakly the system to two sensors or quantized modes (such that the dot dynamics remains unaltered), which model the filtering and detection processes. The intensity–intensity cross correlations of the emission from such sensors, with operators ς_1 and ς_2, provide the two-photon spectrum in a simple form,

$$g_\Gamma^{(2)}(\omega_1; \omega_2, \tau) = \frac{\langle n_1(0)n_2(\tau)\rangle}{\langle n_1(0)\rangle\langle n_2(0)\rangle}, \tag{13}$$

---

[1] One can find its definition in an integral form in [36] (Supplemental material), equation (17).
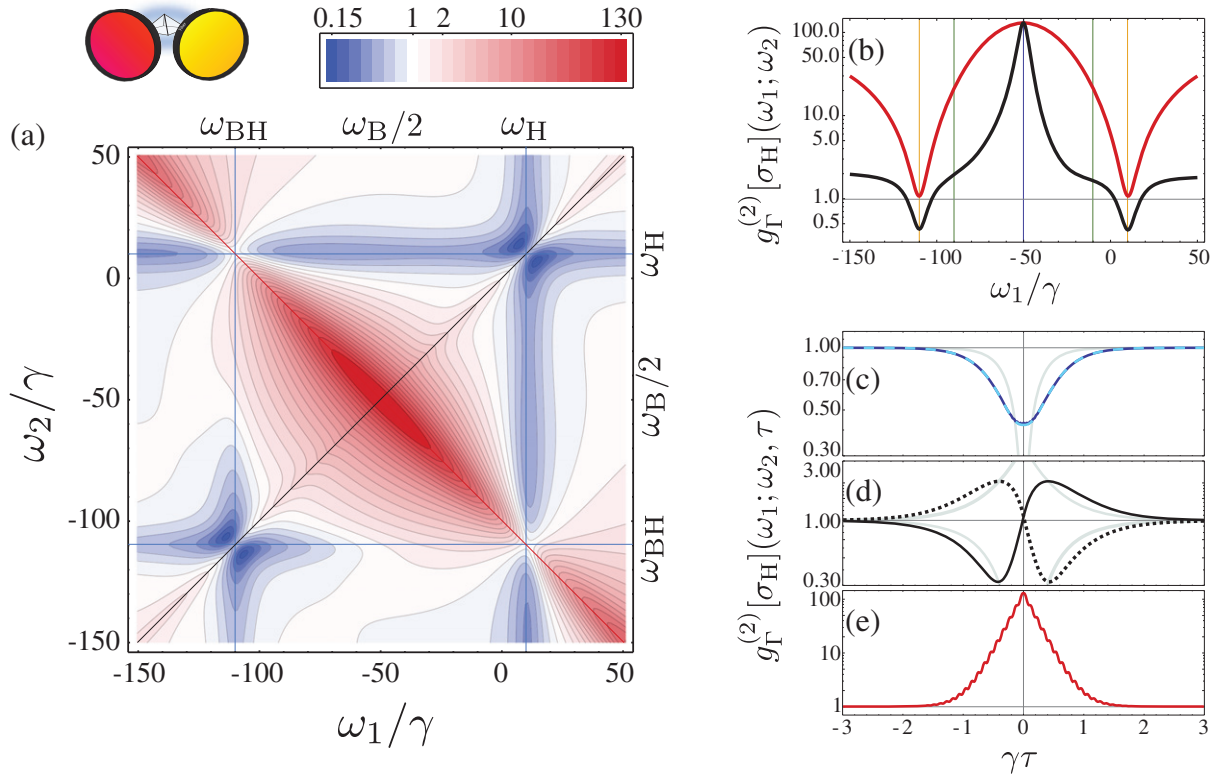
Figure 3. (a) Two-photon spectrum of a quantum dot (with a biexciton structure), with $\Gamma = 5\gamma$. The density plot shows how the correlations between photons are distributed depending on their frequency of emission, from sub-Poissonian ($g_\Gamma^2[\sigma_H](\omega_1;\omega_2) < 1$, in blue) to super-Poissonian (>1, in red) passing by Poissonian ($=1$, in white). The blue 'butterflies' on the diagonal are typical of two-level systems. The antidiagonal corresponds to leapfrog processes with direct emission of two photons through an intermediate virtual state. (b) Cuts from the density plot along the diagonal $\omega_2 = \omega_1$ (in black) and the antidiagonal $\omega_2 = -\chi - \omega_1$ (in red). The diagonal also corresponds to applying a single filter. (c)–(e) Comparison of the τ-dynamics for three cases of interest: (c) antibunching at the heart of the two blue butterflies on the diagonal at ($\omega_{BH}; \omega_{BH}$) (solid dark blue) and ($\omega_H; \omega_H$) (dashed clear blue), (d) cross-correlation of the peaks at ($\omega_{BH}; \omega_H$) (solid) and vice versa, ($\omega_H; \omega_{BH}$) (dotted), showing typical cascade behaviour and (e) the strong bunching at ($\omega_B/2; \omega_b/2$) where two-photon emission is optimum. In (c) and (d), we also plot with pale grey lines the second-order correlations of the corresponding effective operators, equation (12). Scales are logarithmic. Parameters: $P = \gamma$, $\chi = 100\gamma$ and $\delta = 20\gamma$.

where $n_i = \varsigma_i^+\varsigma_i$ for $i = 1, 2$. The sensors natural frequencies, ω_i, decay rates, Γ, and the delay in the detection, τ, can be varied to scan the relevant frequency and time ranges with the appropriate resolution. This method will be applied here for the first time to the case of biexciton emission and used to understand, characterize and enhance various processes useful for its quantum emission. We start by solving the coupling of two sensors with the H-mode only,

obtaining $g_\Gamma^{(2)}[\sigma_H](\omega_1; \omega_2, \tau)$. A detailed discussion on even more fundamental emitters is given in [38].

Experimentally, the two-photon spectrum corresponds to the usual Hanbury Brown–Twiss setup to measure second-order correlations through photon counting, with filters or monochromators being placed in front of the detectors to select two, in general different, frequency windows. The technique has been amply used in the laboratory [15, 16, 22, 42–49], but lacking hitherto a general theoretical description, the global picture provided here has not yet been achieved experimentally. Note finally that when considering correlations between equal frequencies, $\omega = \omega_1 = \omega_2$, the result is equivalent to placing a single filter before measuring the correlations of the outcoming photon stream [36] or embedding the quantum dot in a cavity and measuring the correlations from the emission of a weakly coupled cavity mode with frequency ω.

Figure 3(a) shows the rich landscape provided by the two-photon spectrum $g_\Gamma^{(2)}[\sigma_H](\omega_1; \omega_2)$, in contrast with the one-photon spectrum $S[\sigma_H](\omega)$ and the colour-blind second-order correlations $g^{(2)}[\sigma_H]$, equation (10). It is shown at zero delay ($\tau = 0$), where results are symmetric under exchange of ω_1 and ω_2. An analytical expression is found in this case but it is too lengthy to be reproduced here. The sensor linewidths are chosen to filter the full peaks ($\Gamma = 5\gamma$) in order to observe well-defined regions of enhancement and suppression of the correlations: sub-Poissonian values (<1) are shown in blue, Poissonian ($=1$) in white and super-Poissonian (>1) in red. This figure is the backbone of this paper. We now discuss in turn these different regions where the quantum dot operates as a quantum source with different properties.

3. Distilling single photons and photon pairs

3.1. Single-photon source

When the filters are tuned to the same frequency (diagonal black line in the ($\omega_1; \omega_2$) space in figure 3(a)), there is a systematic enhancement of the bunching as compared to the surrounding regions due to the two possibilities of detecting identical photons [36, 38]. Despite this feature, which is independent of the system dynamics, when both frequencies coincide with one of the dot transitions, ($\omega_H; \omega_H$) or ($\omega_{BH}; \omega_{BH}$), there is a dip in the correlations. This is more clearly shown in the cut at equal frequencies, the black line in figure 3(b). The blue butterfly shape that is observed in the two-photon spectrum locally around each of the dot transitions is characteristic of an isolated two-level system [38]. This zero delay information is complemented by the antibunched τ dynamics, shown in figure 3(c). The two dot resonances, upper and lower, coincide in this case due to the symmetric conditions $P = \gamma$ but they are typically different (the upper level being less antibunched at low pump). Filtering and detection makes it impossible to have a perfect antibunching, getting closest to the ideal correlations $g_\Gamma^{(2)}[\sigma_H](\omega_H; \omega_H, \tau) \approx g^{(2)}[s_1; s_1](\tau)$ from equations (12), at around $\Gamma \approx \chi/2$. At this point, the peaks are maximally filtered with still negligible overlapping of the filters. It is possible to derive a useful expression for the filtered correlations at $\tau = 0$, with $\Gamma \leqslant \chi/2$, in the limit

$$\lim_{\chi \to \infty} g_\Gamma^{(2)}[\sigma_H](\omega_H; \omega_H) = \frac{2(P + \gamma)^2(3P + \gamma + \Gamma)(2\gamma + \Gamma)}{\gamma(P + \gamma + \Gamma)(2P + 2\gamma + \Gamma)(3P + \gamma + 3\Gamma)} \tag{14}$$

typically relevant in experiments.

All this shows that one can recover or optimize the quantum features of a single photon source (antibunching) in a system whose total emission is uncorrelated, by frequency filtering photons from individual transitions. Consequently, the system should exhibit two-photon blockade when probed by a resonant laser at frequency ω_L in resonance with the lower transition, $\omega_L = \omega_H$. The antibunched emission of each of the four filtered peaks of the spectrum has been observed experimentally [15].

3.2. Cascaded two-photon emission

When the filtering frequencies match both the upper and lower quantum-dot transitions, i.e. $(\omega_{BH}; \omega_H)$, the correlations are close to one at zero delay, like for the total emission $g^{(2)}[\sigma_H]$ (which is *exactly* one). However, although the latter is uncorrelated, since it remains equal to one at all τ, the filtered cascade emission is *not* uncorrelated, since it is close to unity only at zero delay and precisely because of strong correlations that are, however, of an opposite nature at positive and negative delays, i.e. showing enhancement for $\tau > 0$ when photons are detected in the natural order that they are emitted, and suppression for $\tau < 0$ when the order is the opposite. This is depicted in figure 3(d) where the solid line corresponds to $(\omega_{BH}; \omega_H)$ and the dotted line to exchanging the filters, $(\omega_H; \omega_{BH})$. As this also corresponds to detecting the photons in the opposite time order, the two curves are exact mirror image of each other.

The identification of the upper and lower transition photons with frequency-blind operators $(g^{(2)}[s_1; s_2](\tau)$ in equations (12)) provides crossed correlations different from our exact and general frequency resolved functions, especially at $\tau = 0$, as shown in figure 3(d), where there is a discontinuity for the approximated functions. The frequency resolved functions have the typical smooth cascade shape that has been observed experimentally [15, 45]. The dynamics at large τ converges to the approximated functions only for $\Gamma \approx \chi/2$.

3.3. Simultaneous two-photon emission

For simultaneous two-photon emission, the strongest feature lies on the antidiagonal (red line) in figure 3(a), which is also shown as the solid red line in figure 3(b). The strong bunching observed here, when both frequencies are far from the system resonances ω_{BH} and ω_H, corresponds to a two-photon deexcitation directly from the biexciton to the ground state without passing by an intermediate real state[2]. Such a two-photon emission, from a Hamiltonian (equation (1)) that does not have a term to describe it, is made possible via an effective virtual state, supported by the interaction with the output fields (or detectors) and revealed by the spectral filtering. As the intermediate virtual state has no fixed energy and only the total energy $\omega_1 + \omega_2 = \omega_B$ needs to be conserved, the simultaneous two-photon emission is observed on the entire antidiagonal (except, again, when touching a resonance, in which case the cascade through real states takes over). We call such processes 'leapfrog' as they jump over the intermediate excitonic state [38]. The largest bunching is found at the central point, $\omega_1 = \omega_2 = \omega_B/2 = -\chi/2$, and at the far-ends $\omega_1 \ll \omega_{BH}$ and $\omega_1 \gg \omega_H$. Among them, the optimal point is that where also the intensity of the two-photon emission is strong. The frequency resolved Mandel Q parameter takes into account

[2] *Real* states denote those forming the Hilbert space of the Hamiltonian at hand and *virtual* states, those provided by the extraneous output modes (in the sensors or detectors) that have been traced out of the dynamics.

both correlations and the strength of the filtered signal [50]:

$$Q_\Gamma(\omega_1; \omega_2) = \sqrt{S_\Gamma(\omega_1) S_\Gamma(\omega_2)} \left[g_\Gamma^{(2)}(\omega_1; \omega_2) - 1 \right], \tag{15}$$

(where also for the single-photon spectra, the detection linewidth, Γ, is taken into account [51]). As expected, $Q_\Gamma[\sigma_H](\omega_1; \omega_2)$ becomes negligible at very large frequencies, far from the resonances of the system, and reaches its maximum at the two-photon resonance, $(\omega_B/2; \omega_B/2)$ (not shown). The latter configuration is therefore the best candidate for the simultaneous and, additionally, indistinguishable, emission of two photons. The bunching is shown in figure 3(e). The small and fast oscillations are due to the effect of one-photon dynamics with the real states but are unimportant for our discussion and would be difficult to resolve experimentally. While the bunching in such a configuration has not yet been observed experimentally, recently, Ota *et al* [24] successfully filtered the two-photon emission from the biexciton with a cavity mode, which corroborates the above discussion.

4. Filtering and enhancing photon-pair emission from the quantum dot via a cavity mode

Large two-photon correlations are the starting point to create a two-photon emission device. When they have been identified, the next step is to increase their efficiency by enhancing the emission at the right operational frequency. The typical way is to Purcell enhance the emission through a cavity mode with the desired polarization (for instance, H) and strongly coupled with the dot transitions (at resonance). Theoretically, this amounts to adding to the master equation (2) a Hamiltonian part that accounts for the free cavity mode (ω_a) and the coupling to the dot (with strength g), in the rotating wave approximation

$$H_{\text{cav}} = \omega_a a^\dagger a + g(a^\dagger \sigma_H + a \sigma_H^\dagger) \tag{16}$$

along with a Lindblad term $\frac{\kappa}{2} \mathcal{L}_a(\rho)$ that accounts for the cavity decay (at rate κ). The cavity emission is typically characterized by its second-order coherence function, $g^{(2)}[a] = \langle a^\dagger a^\dagger a a \rangle / \langle a^\dagger a \rangle^2$.

By placing the cavity mode at the two-photon resonance, $\omega_a = \omega_B/2$, the virtual leapfrog process becomes real as it finds a real intermediate state in the form of a cavity photon. The deexcitation of the biexciton to ground state is thereby enhanced at a rate $\kappa_{2\text{PR}} \approx (4g^2/\chi)^2/\kappa$, producing the emission of two simultaneous and indistinguishable cavity photons at this frequency [31–33]. There is as well some probability that the cavity mediated deexcitation occurs in two steps, through two different cavity photons at frequencies ω_{BH} and ω_H, at the same rate $\kappa_{1\text{PR}} \approx 4g^2\kappa/\chi^2$. The two alternative paths are schematically depicted with curly blue arrows in figure 2(a). The cavity being far from resonance with the dot transitions, the ratio of two- versus one-photon emission can be controlled by an appropriate choice of parameters [32]. We set $g = \kappa = 5\gamma$, to be in strong-coupling regime and have $\kappa_{2\text{P}} = 0.2\gamma > \kappa_{1\text{P}} = 0.05\gamma$, but with a coupling weak enough for the system to emit cavity photons efficiently. The cavity parameters are such that $\kappa > 2P$ and the pump does not disrupt the two-photon dynamics [33]. The two-photon emission indeed dominates over the one-photon emission as seen in figure 2(c), where the cavity spectrum, $S[a](\omega)$, is plotted with a solid line: the central peak, corresponding to the simultaneous two-photon emission, is more intense than the side peaks produced by single photons. A better cavity (smaller κ) does not emit the biexciton photons right away outside the system, but spoils the original (leapfrog) correlations and leads to smaller correlations in the cavity emission $g^{(2)}[a] \to 2$. This is shown in figure 4(a) with a blue solid line. Our previous
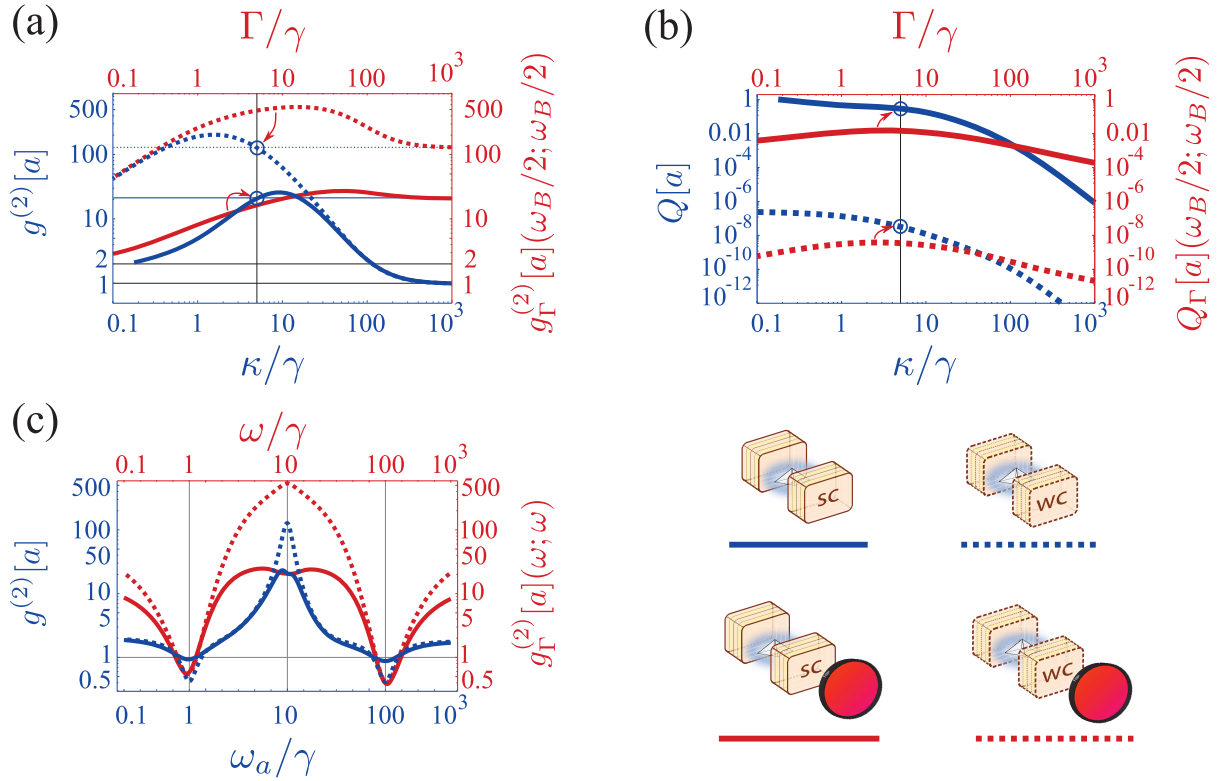
Figure 4. (a) Second-order correlations of a cavity mode embedding a quantum dot in weak (dotted) and strong (solid) coupling. Both the full, colour-blind, cavity emission (in blue) $g^{(2)}[a]$ and the frequency-resolved correlations at the two-photon resonance (in red) $g_\Gamma^{(2)}[a](\omega_B/2; \omega_B/2)$ are considered, with the former relating to the bottom axis (the cavity linewidth κ) and the latter to the upper axis (the detector linewidth Γ) at $\kappa = 5\gamma$ (indicated by a circle). (b) Mandel Q parameter in the same configuration as in (a), supplementing the information of the previous panel with the intensity of the emission. (c) The same as (a) but now as a function of the cavity frequency ω_a (bottom axis) for the colour-blind correlations (in blue) and of the detection frequency ω (upper axis) for the frequency-resolved correlations (in red). Parameters: (a) the strong coupling is for $g = 5\gamma$ and the weak coupling is in the limit of vanishing coupling $g \to 0$ where the cavity is completely equivalent to a filter. Parameters: $P = \gamma$, $\chi = 100\gamma$ and $\delta = 20\gamma$.

choice $\kappa = 5\gamma$, is close to that which maximizes bunching (vertical line in figure 4(a)). A weak coupling due to small coupling strength ($g \to 0$), plotted with a blue dotted line, recovers the case of a filter, discussed in the previous section:

$$\lim_{g \to 0} g^{(2)}[a] = g_\kappa^{(2)}[\sigma_H](\omega_a; \omega_a). \tag{17}$$

The cavity spectrum in this case, plotted with a blue dotted line in figure 2(c), is no longer dominated by the two-photon emission.

Regardless of the coupling strength g (within the validity limits of the rotating wave approximation), the system goes into weak coupling at large enough κ, so both the blue lines,

solid and dotted, converge to the same curve at $\kappa \to \infty$. The cavity then filters the whole dot emission and recovers the total dot correlations for the H-mode, $g^{(2)}[a] \to g^{(2)}[\sigma_H] = 1$. Note that while the bunching in $g^{(2)}[a]$ is better in weak coupling or with a filter, this is at the price of decreasing the enhancement of the emission and, therefore, the efficiency of the quantum device, as the total Mandel $Q[a]$ parameter shows in figure 4(b).

4.1. Distilling the two-photon emission from the cavity field

In view of the preceding results, we now consider the possibility to further enhance the two-photon emission by filtering the cavity photons from the central peak in figure 2(c). That is, we study $g_\Gamma^{(2)}[a](\omega_1; \omega_2)$ for an H-polarized cavity with $\kappa = 5\gamma$ and $\omega_a = \omega_B/2$. In this way, firstly, the cavity acts as a filter, extracting the leapfrog emission where it is most correlated, but also enhances specifically the two-photon emission and, secondly, the filtering of the cavity emission selects only those photons that truly come in pairs. Such a chain is similar to a 'distillation' process where the quantum emission is successively refined.

The results are plotted with red lines in figure 4, for the case $\kappa = 5g$ pinpointed by circles on the blue lines. The filtered cavity emission is indeed generally more strongly correlated at the two-photon resonance than the unfiltered total cavity emission, plotted in blue: $g_\Gamma^{(2)}[a](\omega_B/2; \omega_B/2) \geqslant g^{(2)}[a]$. This is so for all $\Gamma > \kappa$ for the cavity in weak coupling, where the distillation always enhances the correlations. In strong coupling, the filter must strongly overlap with the peak ($\Gamma \gg \kappa$). This is because the side peaks are prominent in weak coupling ($\kappa_{2P} < \kappa_{1P}$), and the filtering efficiently suppresses their detrimental effect, whereas in strong coupling, two-photon correlations are already close to maximum, thanks to the dominant central peak as seen in figure 2(c), and it is therefore important for the filter to strongly overlap with it. In all cases, at large enough Γ, the full cavity correlations are recovered as expected: $\lim_{\Gamma \to \infty} g_\Gamma^{(2)}[a](\omega_1; \omega_2) = g^{(2)}[a]$. In figure 4(a), this means that the red lines converge to the value projected by the circle on the blue lines at $\kappa = 5\gamma$. Here, again, filtering enhances correlations but reduces the number of counts, as shown in figure 4(b).

In figure 4(c), we do the same analysis as in figure 3(b) where there was no distillation. We address the same cases but now as a function of frequency, fixing the cavity decay rate $\kappa = 5\gamma$ and the filtering linewidth at $\Gamma = 10\gamma$. In blue, we consider the cavity QED case in weak and strong coupling, without filtering. Since the weak-coupling limit is identical to the single filter case, note that the blue dotted line in figure 4(c) is identical to the black solid line in figure 3(b). Off-resonance, the cavity acts as a simple filter due to the reduction of the effective coupling. The stronger coupling to the cavity has an effect only when involving the real states, where it spoils the correlations, less bunched at the two-photon resonance $\omega_a = \omega_B/2$ and less antibunched at the one-photon resonances, $\omega_a = \omega_{BH}$ or $\omega_a = \omega_H$. This shows again that useful quantum correlations are obtained in a system where quantum processes are Purcell enhanced and quickly transferred outside, rather than stored and Rabi-cycled over within the cavity. The same is true for the red line, further filtering the output. Finally, comparing solid lines together, we see again that there is little if anything to be gained by filtering in strong coupling, whereas in weak coupling, the enhancement is considerable. As a summary, the filtering of the weakly coupled cavity (red dotted) provides the strongest correlations (at the cost of the available intensity), corresponding to distilling the photon pairs out of the original dot spectrum without any additional enhancement.

In figure 5, we show the full two-photon spectra for a quantum dot in a cavity, in both (a) strong and (b) weak coupling. The antibunching regions on the diagonal and the bunching
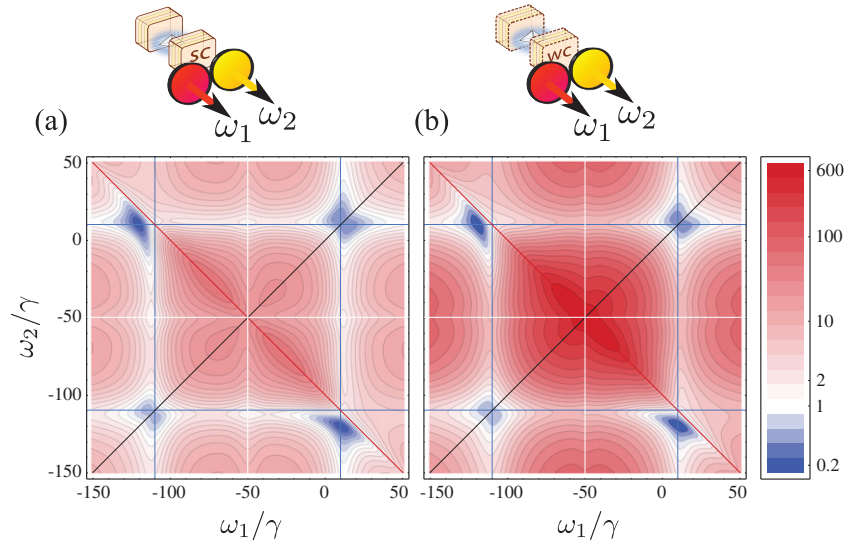
Figure 5. Two-photon spectra $g_\Gamma^{(2)}[a](\omega_1; \omega_2)$ for a quantum dot in a cavity in the (a) strong-, $g = \kappa$, and (b) weak-coupling regime, when the cavity is at the two-photon resonance, $\omega_a = \omega_B/2$. The bunching regions are strengthened by the cavity (the total, colour-blind correlations are $g^{(2)}[a] \approx 21$ for (a) and 130 for (b)). Horizontal and vertical structure also emerges at the two-photon resonance (white lines), betraying the presence of real states. These are stronger, the stronger the coupling. Parameters: $\kappa = 5\gamma$, $P = \gamma$, $\chi = 100\gamma$, $\delta = 20\gamma$ and $\Gamma = 10\kappa$.

along the antidiagonal are qualitatively similar to the filtered dot emission, but antibunching is milder and less extended in contrast to bunching that greatly dominates the two-photon spectrum as a direct consequence of the cavity. At the central point, bunching is now, respectively, weaker (stronger) than the filtered dot emission, due to the saturated (efficient) distillation in strong (weak) coupling. Another striking feature added by the cavity is the appearance of an additional pattern of horizontal and vertical lines at ω_a. While diagonal and antidiagonal features correspond to virtual processes horizontal and vertical stem from real processes that pin the correlations at their own frequency. Therefore, the new features are a further illustration that the two-photon emission becomes a real resonance of the cavity–dot system, in contrast with figure 3(a) where it was virtual. The effect is more pronounced in the strong-coupling regime since this is the case where the new state is better defined. Another qualitative difference between figures 5 and 3(a) is in the regions surrounding the cascade configuration, $(\omega_{BH}; \omega_H)$, which has changed shape to become two antibunching blue spots. This is due to the fact that the single-photon cascade is much less likely to happen through the cavity mode than the direct deexcitation of the dot, as $\kappa_{1P} = 0.05\gamma \ll \gamma$. Even if the first photon from the biexciton emission decays through the cavity, the second will most likely not.

5. Distilling entangled photon pairs

One of the most sophisticated applications of the biexciton structure in a quantum dot is as a source of polarization entangled photon pairs [15, 16, 21, 35, 52–61]. Without the fine-structure splitting, $\delta = 0$, the two possible two-photon deexcitation paths are indistinguishable except

for their polarization degree of freedom (H or V), producing equal frequency photon pairs $(\omega_{BX}; \omega_X)$, with $\omega_{BX} = \omega_B - \omega_X$. This results in the polarization entangled state

$$|\psi\rangle = \frac{1}{\sqrt{2}}(|H(\omega_{BX}), H(\omega_X)\rangle + e^{-i\phi} |V(\omega_{BX}), V(\omega_X)\rangle). \tag{18}$$

The splitting δ provides 'which path' information [62] that spoils indistinguishability, producing a state entangled in both frequency and polarization [34]:

$$\left|\psi'\right\rangle = \frac{1}{\sqrt{2}}(|H(\omega_{BH}), H(\omega_H)\rangle + e^{-i\phi'} |V(\omega_{BV}), V(\omega_V)\rangle). \tag{19}$$

Although these doubly entangled states are useful for some quantum applications [63, 64], it is typically desirable to erase the frequency information and recover polarization-only entangled pairs. Among other solutions, such as cancelling the built-in splitting externally [16, 65], filtering has been implemented with $\omega_1 = \omega_{BX}$ and $\omega_2 = \omega_X$ to make the pairs identical in frequencies again [15, 34, 54], at the cost of increasing the randomness of the source (making it less 'on-demand'). Recently, the cavity filtering of the polarization entangled photon pairs with $\omega_a = \omega_B/2$ was proposed by Schumacher *et al* [35] taking advantage of the additional two-photon enhancement [32]. Let us revisit these effects in the light of the previous results.

5.1. Characterization of the filtered entangled photon-pair emission

The properties of the output photons can be obtained from the two-photon state density matrix, $\theta(\tau)$, reconstructed in the basis $\{|H1, H2\rangle, |H1, V4\rangle, |V3, H2\rangle, |V3, V4\rangle\}$, denoting by $|xi\rangle$ with $x =$H or V and $i = 1, 2, 3, 4$, the state $|x(\omega_i)\rangle$. The frequencies ω_i are, in general, different. The second photon is detected with a delay τ with respect to the first one (detected in the steady state). Let us express this matrix in terms of frequency resolved correlators, as is typically done in the literature [53, 55]. However, in contrast to previous approaches, we do not identify the photons with the transition from which they may come (using the dot operators $|G\rangle \langle x|$, $|x\rangle \langle B|$ with, again, x standing for either H or V) but with their measurable properties, that is, polarization, frequency and time of detection (for a given filter window). This is a more accurate description of the experimental situation where a given photon can come from any dot transition and any transition can produce photons at any frequency and time with some probability. We describe the experiments by considering four different filters, that is, including all degrees of freedom of the emitted photons in the description. Each detected filtered photon corresponds to the application of the filter operator ς_j with $j =$H1, H2, V3, V4 corresponding to its coupling to the H or V dot transitions with ω_i frequencies. Then, the two-photon matrix $\theta'_\Gamma(\tau)$ (the prime refers to the lack of normalization) corresponding to a tomographic measurement is theoretically modelled as

$$\theta'_\Gamma(\tau) = \begin{pmatrix} \langle n_{H1}(0)n_{H2}(\tau)\rangle & \langle n_{H1}(0)[\varsigma_{H2}^+\varsigma_{V4}](\tau)\rangle & \langle[\varsigma_{H1}^+\varsigma_{V3}](0)n_{H2}(\tau)\rangle & \langle[\varsigma_{H1}^+\varsigma_{V3}](0)[\varsigma_{H2}^+\varsigma_{V4}](\tau)\rangle \\ \text{h.c.} & \langle n_{H1}(0)n_{V4}(\tau)\rangle & \langle[\varsigma_{H1}^+\varsigma_{V3}](0)[\varsigma_{V4}^+\varsigma_{H2}](\tau)\rangle & \langle[\varsigma_{H1}^+\varsigma_{V3}](0)n_{V4}(\tau)\rangle \\ \text{h.c.} & \text{h.c.} & \langle n_{V3}(0)n_{H2}(\tau)\rangle & \langle n_{V3}(0)[\varsigma_{H2}^+\varsigma_{V4}](\tau)\rangle \\ \text{h.c.} & \text{h.c.} & \text{h.c.} & \langle n_{V3}(0)n_{V4}(\tau)\rangle \end{pmatrix} \tag{20}$$

where $n_i = \varsigma_i^+\varsigma_i$ (we have dropped the frequency dependence in the notation, writing $\theta'_\Gamma(\tau)$ instead of $\theta'_\Gamma(\omega_1, \omega_2; \omega_3, \omega_4, \tau)$). Since a weakly coupled cavity mode behaves as a filter, this tomographic procedure is equivalent to considering the four dot transitions coupled to four

different cavity modes with the corresponding polarizations, central frequencies and decay rates [35, 61]. Unlike in other works where for various reasons and particular cases, some of the elements in $\theta'_\Gamma(\tau)$ are set to zero or considered equal, here we keep the full matrix with no *a priori* assumptions since, in general, it may not reduce to a simpler form due to the incoherent pumping, pure dephasing, frequency filtering and fine-structure splitting.

There are essentially two ways to quantify the degree of entanglement from the density matrix $\theta'_\Gamma(\tau)$. The most straightforward is to consider the τ-dependent matrix directly, which merely requires normalization at each time τ, yielding $\theta_\Gamma(\tau) = \theta'_\Gamma(\tau)/\mathrm{Tr}[\theta'_\Gamma(\tau)]$. The physical interpretation is that of photon pairs emitted with a delay τ, that is, within the time resolution $1/\Gamma$ of the filter or cavity [34, 61]. In particular, the zero-delay matrix, $\theta_\Gamma(0)$, represents the emission of two *simultaneous* photons [59, 60]. The second approach is closer to the experimental measurement which averages over time. In this case, one considers the integrated quantity $\Theta_\Gamma(\tau_{\max}) = (\int_0^{\tau_{\max}} \theta'_\Gamma(\tau)\,\mathrm{d}\tau)/\mathcal{N}$ that averages over all possible emitted pairs from the system [15, 53]. It is also normalized (by $\mathcal{N}$), but after integration, so that the two approaches are not directly related to each other and present alternative aspects of the problem, discussed in detail in the following. Without the cutoff delay $\tau_{\max}$, the integral diverges due to the continuous pumping.

The degree of entanglement of any bipartite system represented by a 4×4 density matrix θ can be quantified by the *concurrence*, C, which ranges from 0 (separable states) to 1 (maximally entangled states)[3] [66]. High values of the concurrence require high degrees of purity in the system [67], it being, for instance, impossible to extract any entanglement from a maximally mixed state (in which case all the four basis states occur with the same probability). The filtered density matrices, $\Theta_\Gamma(\tau_{\max})$ and $\theta_\Gamma(\tau)$, provide each their own concurrence that we will denote by $C_\Gamma^{\mathrm{int}}(\tau_{\max})$ and $C_\Gamma(\tau)$, respectively.

5.2. Comparison between different filtering configurations

We begin by considering the standard cascade configuration by detecting photons at the dot resonances, i.e. $\omega_1 = \omega_{\mathrm{BH}}$, $\omega_2 = \omega_{\mathrm{H}}$, $\omega_3 = \omega_{\mathrm{BV}}$, $\omega_4 = \omega_{\mathrm{V}}$, as sketched in the inset of figure 6(a). The upper density plot shows $C_\Gamma^{\mathrm{int}}(\tau_{\max})$ and the density plot below shows the time-resolved concurrence $C_\Gamma(\tau)$, as a function of $\tau_{\max}$ or τ and δ, for $\Gamma = 2\gamma$. The two concurrences, $C_\Gamma^{\mathrm{int}}(\tau_{\max})$ and $C_\Gamma(\tau)$, are qualitatively different except at $\tau = \tau_{\max} = 0$ where they are equal by definition. They also have in common that the maximum concurrence is not achieved at zero delay (it is most visible as the darker red area around $(\gamma\tau_{\max}, \delta/\gamma) \approx (0.4, 0)$). This is because this filtering scheme relies on the real-states deexcitation of the dot levels, and thus exhibits the typical delay from the cascade-type dynamics of correlations (see figure 3(d)). The major departure between the two is that the decay of $C_\Gamma^{\mathrm{int}}(\tau_{\max})$ is strongly dependent on δ, while $C_\Gamma(\tau)$ is not. With no splitting, at $\delta = 0$, the ideal symmetrical four-level structure efficiently produces the entangled state $|\psi\rangle$ and the concurrence is maximum both for the integral and the time-resolved forms. The decay time of $C_\Gamma(\tau)$ is the simplest to understand as, when filtering full peaks, it is merely related to the reloading time of the biexciton, of the order of the inverse pumping rate, $\sim 2/P$ [61]. The asymmetry due to a non-zero splitting in the four-level system causes an unbalanced dynamics of deexcitation via the H and V polarizations. The entanglement in the form $|\psi\rangle$ is downgraded to $|\psi'\rangle$. The fact that the concurrence $C_\Gamma(\tau)$

---

[3] Its definition reads $C \equiv [\max\{0, \sqrt{\lambda_1} - \sqrt{\lambda_2} - \sqrt{\lambda_3} - \sqrt{\lambda_4}\}]$, where $\{\lambda_1, \lambda_2, \lambda_3, \lambda_4\}$ are the eigenvalues in decreasing order of the matrix $\theta T \theta^* T$, with T an antidiagonal matrix with elements $\{-1, 1, 1, -1\}$.
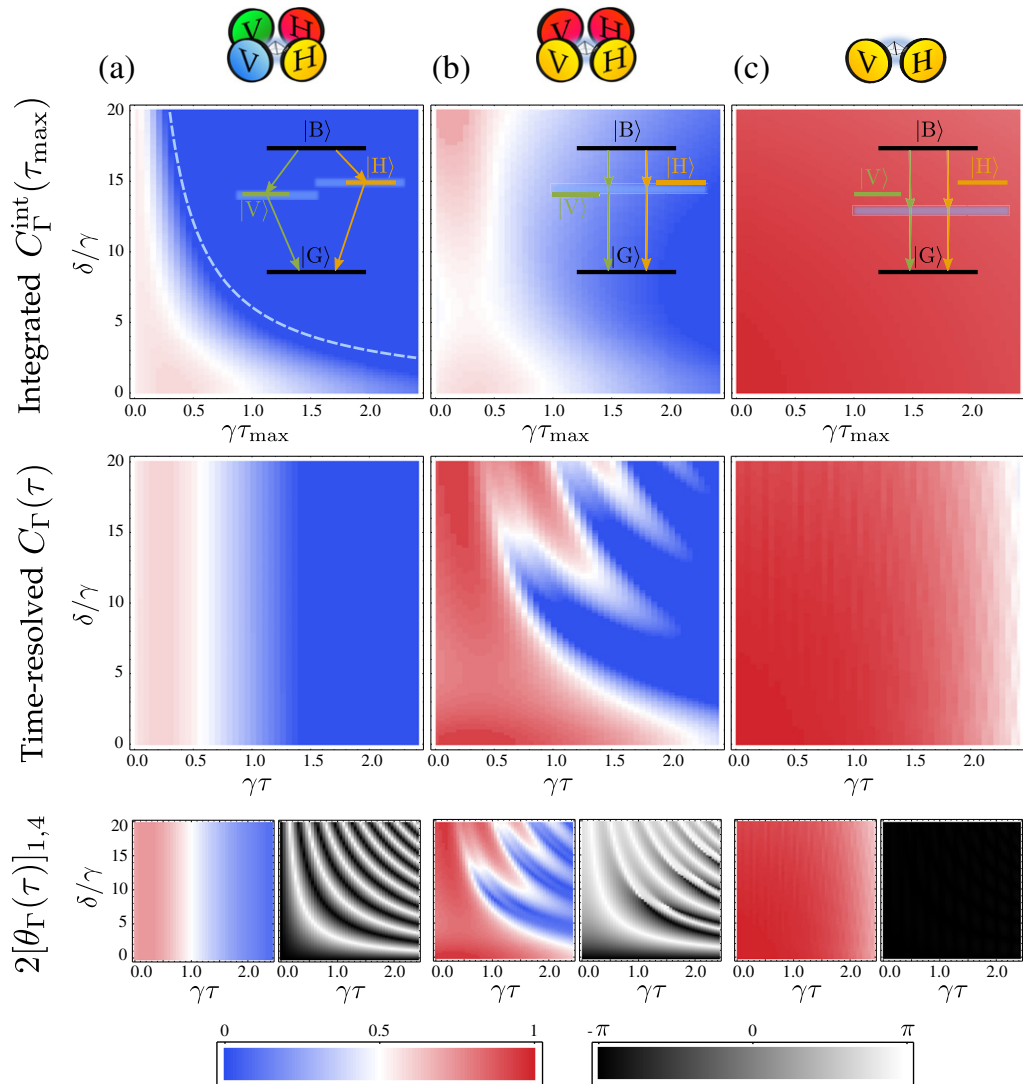
Figure 6. Concurrence for three different schemes of entanglement distillation (as sketched above each column): (a) filtering the four different dot resonances in their cascade through the real states, (b) filtering at two different frequencies $\omega_1 = \omega_{BX}$ and $\omega_2 = \omega_X$, degenerate in both polarization decay paths, (c) filtering at the same frequency $\omega_B/2$, i.e. at the two-photon resonance. The upper panels show the time-integrated concurrence $C_\Gamma^{int}(\tau_{max})$ as a function of its cutoff τ_{max} and the fine-structure splitting δ. In (a), the line $\tau_{max} = 2\pi/\delta$ bounding the region with entanglement is superimposed. The intermediate panels show the instantaneous concurrence $C_\Gamma(\tau)$ as a function of delay and splitting. The lowest panels show (twice) the modulus and phase of the off-diagonal element $[\theta_\Gamma(\tau)]_{1,4}$ typically used in the literature to quantify entanglement. All these plots show that as far as the degree of entanglement is concerned, the leapfrog emission is the best configuration and is optimum at the two-photon resonance. Parameters: $P = \gamma$, $\chi = 100\gamma$ and $\Gamma = 2\gamma$.

is not affected shows that it accounts for the degree of entanglement in both polarization and frequency, which is oblivious to the 'which path' information that the last variable provides. On the other hand, $C_\Gamma^{\mathrm{int}}(\tau_{\max})$ is suppressed by the splitting as fast as $\tau_{\max} > 2\pi/\delta$ (this boundary is superimposed on the density plot). That is, as soon as the integration interval is large enough to resolve it. The integrated $C_\Gamma^{\mathrm{int}}(\tau_{\max})$, therefore, accounts for the degree of entanglement in polarization only, and is destroyed by the 'which path' information provided by the different frequencies. The exact mechanism at work to erase the entanglement is shown in the lower row of figure 6, which displays the upper right matrix element $[\theta_\Gamma(\tau)]_{1,4}$ of the density matrix, which is most responsible for purporting entanglement. The modulus is shown on the left (with blue meaning 0 and red meaning 0.5) and the phase on the right (in black and white). The time-resolved concurrence $C_\Gamma(\tau)$ is very similar to the modulus of $[\theta_\Gamma(\tau)]_{1,4}$ which justifies the approximation often made in the literature $C_\Gamma(\tau) = 2(|[\theta_\Gamma(\tau)]_{1,4}| - [\theta_\Gamma(\tau)]_{2,2})$ with $[\theta_\Gamma(\tau)]_{2,2}$ small [53]. Although each photon pair is entangled, it is so in the state $|\psi'\rangle$ with a phase, $\phi' = -\pi + \delta\tau$, that accumulates with τ at a rate δ [34], but this does not matter as far as instantaneous entanglement is concerned, and this is why the splitting does not affect $C_\Gamma(\tau)$. On the other hand, when integrating over time, the varying phase, which completes a 2π-cycle at intervals $2\pi/\delta$, randomizes the quantum superposition and results in a classical mixture. This is why the splitting does completely destroy $C_\Gamma^{\mathrm{int}}(\tau_{\max})$ for $\tau_{\max} > 2\pi/\delta$. And this is how the system restores the 'which path' information: given enough time, if the splitting is large enough, the photons lose their quantum coherence due to the averaging out of the relative phase between them because of their distinguishable frequency.

Another possible configuration proposed in the literature [15, 34, 54] is sketched in the inset of figure 6(b). Photons are detected at the frequency that lies between the two polarizations, $\omega_1 = \omega_3 = \omega_{\mathrm{BX}}$, $\omega_2 = \omega_4 = \omega_{\mathrm{X}}$. For small splittings, the entanglement production scheme still relies on the cascade and real deexcitation of the dot levels. Therefore, the behaviour of $C_\Gamma^{\mathrm{int}}(\tau_{\max})$ is similar to (a) (decaying with δ) but slightly improved by the fact that the contributions to the density matrix are more balanced by filtering in between the levels. For splittings large enough to allow the formation of leapfrog emission in both paths, $\delta \gg \Gamma$, there is a striking change of trend and $C_\Gamma^{\mathrm{int}}(\tau_{\max})$ remains finite at longer delays $\tau_{\max}$ when increasing δ. This is a clear sign that the entanglement relies on a different type of emission, namely simultaneous leapfrog photon pairs, rather than a cascade through real states. Accordingly, the intensity is reduced as compared to that obtained at smaller δ or to the non-degenerate cascade in (a), but the bunching is stronger, as evidenced by the two-photon spectrum, and results in a larger degree of entanglement than at $\delta = 0$. A similar result is obtained qualitatively with the time-resolved concurrence, a strong resurgence of entanglement with δ, indicating again very high correlations in this configuration. Note finally that the phase becomes much more constant with increasing δ, resulting in the persistence of the correlation in the time-integrated concurrence. This is because the two-photon emission is through the leapfrog processes. Since the latter, by definition, involve intermediate virtual states that are degenerate in frequency, this is a built-in mechanism to suppress the splitting and not suffer from the 'which path' information as when passing through the real states.

Finally, a configuration proposed more recently in the literature [35] is the two-photon resonance, with four equal frequencies, $\omega_1 = \omega_2 = \omega_3 = \omega_4 = \omega_{\mathrm{B}}/2$, as sketched in the inset of figure 6(c). This provides a two-photon source in both polarizations that can be enhanced via two cavity modes with orthogonal polarizations [32]. Remarkably, in this case, the splitting has almost no effect on the degree of entanglement, which is maximum. Here, the leapfrog
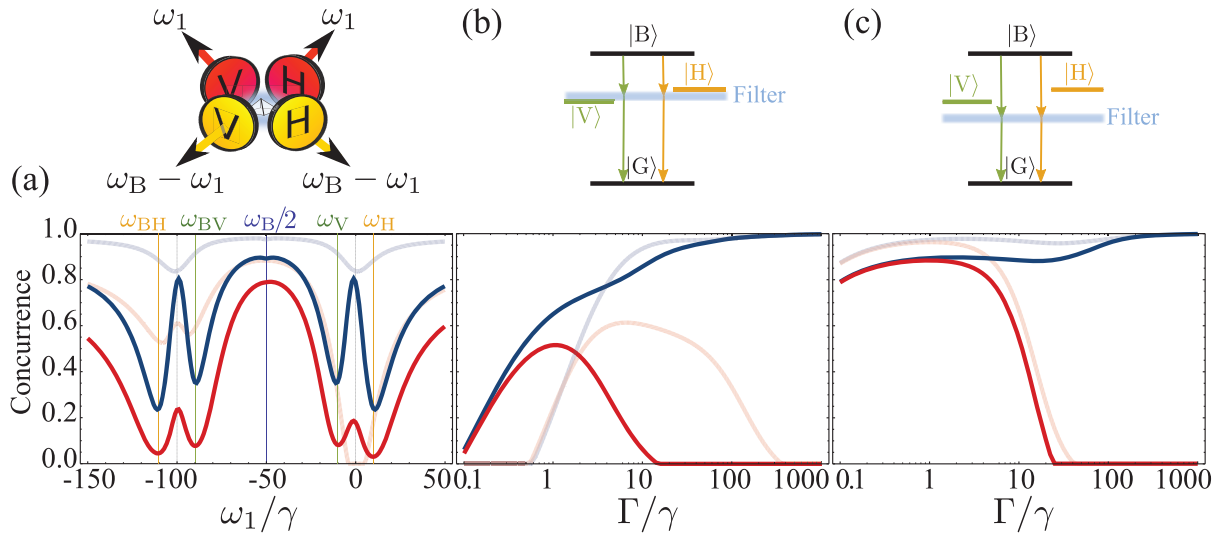
Figure 7. Concurrence computed with the instantaneous emission at $\tau = 0$ (blue) or integrated up to $\tau_{\max} = 1/\gamma$ (red). (a) Plotted for a fixed filter linewidth $\Gamma = 5\gamma$ as a function of the filter frequencies (ω_1; $\omega_B - \omega_1$). The concurrence is high unless a real state is probed and a cascade through it overtakes the leapfrog emission. The optimum case is the two-photon resonance. (b), (c) Plotted as a function of the filter linewidth Γ for the two cases that maximize entanglement in (a), that is, at (b) the degenerate cascade configuration (ω_{BX}; ω_X) and (c) the biexciton two-photon resonance ($\omega_B/2$; $\omega_B/2$). The concurrence of the ideal case at $\delta = 0$ is also plotted as a reference with softer solid lines. Parameters: $P = \gamma$, $\chi = 100\gamma$ and $\delta = 20\gamma$. $\omega_X = 0$ is set as the reference frequency.

mechanism plays at its full extent: the virtual states, on top of being degenerate and thus immune to the splitting, remain always far, and are therefore protected, from the real states. This results in the exactly constant phase (black panel on the lower right end of figure 6). As a result, both $C_\Gamma^{\text{int}}(\tau_{\max})$ and $C_\Gamma(\tau)$ remain large. The only drawback of this mechanism is, being virtual-processes mediated, a comparatively weaker intensity.

5.3. Filtering the leapfrog emission

We conclude with a more detailed analysis of what appears to be the most suitable scheme to create robust entanglement, the leapfrog photon-pair emission. The target state is always $|\psi\rangle$, equation (18), due to the degeneracy in the filtered paths. The concurrence is shown as a function of the first photon frequency, ω_1, in figure 7 (the second photon has the energy $\omega_2 = \omega_B - \omega_1$ to conserve the total biexciton energy). The time-integrated (resp. instantaneous) concurrence $C_\Gamma^{\text{int}}(1/\gamma)$ (resp. $C_\Gamma(0)$) is shown in red (resp. blue) lines, both for a large splitting $\delta = 20\gamma$ in strong tones and for $\delta = 0$ in softer tones. In the first panel, (a), the frequency ω_1 of the filters is varied. This figure shows that concurrence is very high (with high state purity) when the filtering frequencies are far from the system resonances: $\omega_{BH/BV}$ and $\omega_{H/V}$. These are shown as coloured grid lines to guide the eye. In this case, the real states are not involved and the leapfrog emission is efficient in both polarizations. The concurrence otherwise drops when ω_1 is resonant with any one-photon transition, meaning that photons are then emitted in a cascade in one of the polarizations, rather than simultaneously through a leapfrog process. Moreover, if at least one of

the two deexcitation paths is dominated by the real state dynamics, this brings back the problem of 'which path' information, which spoils indistinguishability and entanglement. There is only one exception to this general rule, namely, the $\delta = 0$ integrated case (soft red line) which has a local maximum at ω_{BX}, i.e. when touching its resonance in the natural cascade order. This is because the paths are anyway identical and the integration includes the possibility of emitting the second photon with some delay (up to τ_{max}). For the case of $\delta \neq 0$, if this is large enough, it is still possible to recover identical paths while filtering the leapfrog in the middle points, $\omega_1 = \omega_{BX}$ and $\omega_2 = \omega_X$, to produce entangled pairs.

Overall, the optimum configuration is, therefore, indeed at the middle point $\omega_1 = \omega_2 = \omega_B/2$ (two-photon resonance), where the photons are emitted simultaneously, with a high purity, and entanglement degrees are also identical in frequency by construction. Entanglement is also always larger in the simultaneous concurrence (blue lines) as this is the natural choice to detect the leapfrog emission, which is a fast process. This comes at the price, expectedly, of decreasing the total number of useful counts and increasing the randomness of the source. Note finally that the blue curves are symmetric around $\omega_B/2$, but the red ones are not, given that in the integrated case, the order of the photons with different frequencies is relevant. The left-hand side of the plot, $\omega_1 < \omega_B/2$, corresponds to the natural order of the frequencies in the cascade, $\omega_1 < \omega_2$. The opposite order, being counter-decay, is detrimental to entanglement.

Since of all leapfrog configurations, those in figure 6(b) and (c) are optimum to obtain high degrees of entanglement, we provide their dependence on the filter linewidths, Γ, in figures 7(b) and (c). First, we observe that in the limit of small linewidths for the filters, i.e. in the region $\Gamma < 1/\tau_{max}$, the simultaneous and time-integrated concurrences should converge to each other, since the time resolution becomes larger than the integration time. Therefore, the integrated emission provides the maximum entanglement when the frequency window is small enough to provide the same results as the simultaneous emission. Decreasing Γ below P (which in this case is also $P = \gamma$) results in a time resolution in the filtering larger than the pumping timescale $1/P$. Therefore, photons from different pumping cycles start to get mixed with each other. As a result C drops for $\Gamma < \gamma$ in all cases. In the limit $\Gamma \ll P$, the emission is completely uncorrelated and $C = 0$. This is an important difference from the cases of pulsed excitation or the spontaneous decay of the system from the biexciton state. In the absence of a steady state, entanglement is maximized with the smallest window, $\Gamma \to 0$ [15, 54]. Two opposite types of behaviour are otherwise observed in these figures when increasing the filter linewidth and $\Gamma > 1/\tau_{max}$. The simultaneous emission gains in its degree of entanglement, whereas the time-integrated one loses with increasing linewidth. In the limit $\Gamma \to \infty$, this disparity is easy to understand. We recover the colour blind result in all filtering configurations, (b) or (c), that is, the decay of entanglement: from 1 corresponding to $|\psi\rangle$ at $\tau = 0$, to 0 corresponding to a maximally mixed state at large τ. Therefore, $C_\Gamma(0) \to C(0) = 1$ and $C_\Gamma^{int}(\tau_{max}) \to C^{int}(\tau_{max}) = 0$ (for our particular choice of τ_{max} and P).

The decrease in $C_\Gamma^{int}(\tau_{max})$ with increasing filtering window, has been discussed in the literature for the case in figure 7(b) [15, 54], and it has been attributed to a gain of 'which path' information due to the overlap of the filters with the real excitonic levels. In the light of our results, when $\Gamma > \delta$ the real-state deexcitation takes over the leapfrog and $C_\Gamma^{int}(\tau_{max})$ is suppressed indeed due to such a gain of 'which path' information, as discussed previously. However, we find another reason why $C_\Gamma^{int}(\tau_{max})$ decreases with Γ in all cases, based on the leapfrog emission: the region $1/P < \Gamma < \delta$ for case (b) and the region $1/P < \Gamma < \chi$ for case (c). The maximum delay in the emission of the second photon in a leapfrog processes is

related to $1/\Gamma$, due to its virtual nature. Therefore, the initial enhancement of entanglement starts to drop at delays $\tau \approx 1/\Gamma$, after which the emission of a second photon is uncorrelated to the first one (not belonging to the same leapfrog pair). For a fixed cutoff τ_{max}, this leads to a reduction of $C_{\Gamma}^{\mathrm{int}}(\tau_{\mathrm{max}})$ with Γ. Broader filters have a smaller impact on the case of real-state deexcitation (see the zero splitting case in figure 7(b), plotted in soft red), since the system dynamics is slower than the filtering (γ, $P < \Gamma$), the filter merely emits the photons faster and faster after receiving them from the system. This results in a mild reduction of $C_{\Gamma}^{\mathrm{int}}(\tau_{\mathrm{max}})$ with Γ until the detection becomes colour blind and it drops to reach its aforementioned limit of zero.

6. Conclusions

In summary, we have characterized the emission of a quantum dot modelled as a system able to accommodate two excitons of different polarization and bound as a biexciton. Beyond the usual single-photon spectrum (or photoluminescence spectrum), we have presented for the first time the two-photon spectrum of such a system, and discussed the physical processes unravelled by frequency-resolved correlations and how they shed light on various mechanisms useful for quantum information processing.

We relied on the recently developed formalism [36] that allows us to compute conveniently such correlations resolved both in time and frequency. This describes both the application of external filters before the detection or due to one or many cavity modes in weak coupling with the emitter. Filters and cavities have their respective advantages, and when combined, can perform a distillation of the emission, by successive filtering that enhances the correlations and purity of the states.

We addressed three different regimes of operation depending on the filtering scheme, namely as a source of single photons, a source of two-photon states (both through cascaded photon pairs and simultaneous photon pairs) and a source of polarization entangled photon pairs, for which a form of the density matrix that is close to the experimental tomographic procedure was proposed. In particular, the so-called leapfrog processes—where the system undergoes a direct transition from the biexciton to the ground state without passing by the intermediate real states but jumping over them through a virtual state—have been identified as key, both for two-photon emission and for entangled photon-pair generation. In the latter case, this allows us to cancel the notoriously detrimental splitting between the real exciton states that spoils entanglement through 'which path' information, since the intermediate virtual states have no energy constraints and are always perfectly degenerate. Entanglement is long-lived and much more robust against this splitting than when filtering at the system resonances. At the two-photon resonance, degrees of entanglement higher than 80% can be achieved and maintained for a wide range of parameters.

Acknowledgments

References

[1] Strauf S, Stoltz N G, Rakher M T, Coldren L A, Petroff P M and Bouwmeester D 2007 High-frequency single-photon source with polarization control *Nature Photon.* **1** 704
[2] Nguyen H S, Sallen G, Voisin C, Roussignol Ph, Diederichs C and Cassabois G 2011 Ultra-coherent single photon source *Appl. Phys. Lett.* **99** 261904

[3] Matthiesen C, Vamivakas A N and Atatüre M 2012 Subnatural linewidth single photons from a quantum dot *Phys. Rev. Lett.* **108** 093602

[4] Boyle S J, Ramsay A J, Fox A M and Skolnick M S 2009 Beating of exciton-dressed states in a single semiconductor InGaAs/GaAs quantum dot *Phys. Rev. Lett.* **102** 207401

[5] Vamivakas A N, Zhao Y, Lu C-Y and Atatüre M 2009 Spin-resolved quantum-dot resonance fluorescence *Nature Phys.* **5** 198

[6] Ramsay A J 2010 A review of the coherent optical control of the exciton and spin states of semiconductor quantum dots *Semicond. Sci. Technol.* **25** 103001

[7] Simon C M *et al* 2011 Robust quantum dot exciton generation via adiabatic passage with frequency-swept optical pulses *Phys. Rev. Lett.* **106** 166801

[8] Wu Y, Piper I M, Ediger M, Brereton P, Schmidgall E R, Eastham P R, Hugues M, Hopkinson M and Phillips R T 2011 Population inversion in a single InGaAs quantum dot using the method of adiabatic rapid passage *Phys. Rev. Lett.* **106** 067401

[9] Chen G, Stievater T H, Batteh E T, Li X, Steel D G, Gammon D, Katzer D S, Park D and Sham L J 2002 Biexciton quantum coherence in a single quantum dot *Phys. Rev. Lett.* **88** 117901

[10] Flissikowski T, Betke A, Akimov I A and Henneberger F 2004 Two-photon coherent control of a single quantum dot *Phys. Rev. Lett.* **92** 227401

[11] Stufler S, Machnikowski P, Ester P, Bichler M, Axt V M, Kuhn T and Zrenner A 2006 Two-photon Rabi oscillations in a single In$_x$Ga$_{1-x}$As/GaAs quantum dot *Phys. Rev.* B **73** 125304

[12] Akimov I A, Andrews J T and Henneberger F 2006 Stimulated emission from the biexciton in a single self-assembled II–VI quantum dot *Phys. Rev. Lett.* **96** 067401

[13] Boyle S J, Ramsay A J, Fox A M and Skolnick M S 2010 Two-color two-photon Rabi oscillation of biexciton in single InAs/GaAs quantum dot *Physica* E **42** 2485

[14] Miyazawa T, Kodera T, Nakaoka T, Watanabe K, Kumagai N, Yokoyama N and Arakawa Y 2010 Two-photon control of biexciton population in telecommunication-band quantum dot *Appl. Phys. Express* **3** 064401

[15] Akopian N, Lindner N H, Poem E, Berlatzky Y, Avron J, Gershoni D, Gerardot B D and Petroff P M 2006 Entangled photon pairs from semiconductor quantum dots *Phys. Rev. Lett.* **96** 130501

[16] Stevenson R M, Young R J, Atkinson P, Cooper K, Ritchie D A and Shields A J 2006 A semiconductor source of triggered entangled photon pairs *Nature* **439** 179

[17] Hafenbrak R, Ulrich S M, Michler P, Wang L, Rastelli A and Schmidt O G 2007 Triggered polarization-entangled photon pairs from a single quantum dot up to 30 K *New J. Phys.* **9** 315

[18] Reithmaier J P, Sek G, Löffler A, Hofmann C, Kuhn S, Reitzenstein S, Keldysh L V, Kulakovskii V D, Reinecker T L and Forchel A 2004 Strong coupling in a single quantum dot–semiconductor microcavity system *Nature* **432** 197

[19] Yoshie T, Scherer A, Heindrickson J, Khitrova G, Gibbs H M, Rupper G, Ell C, Shchekin O B and Deppe D G 2004 Vacuum Rabi splitting with a single quantum dot in a photonic crystal nanocavity *Nature* **432** 200

[20] Peter E, Senellart P, Martrou D, Lemaître A, Hours J, Gérard J M and Bloch J 2005 Exciton–photon strong-coupling regime for a single quantum dot embedded in a microcavity *Phys. Rev. Lett.* **95** 067401

[21] Dousse A, Suffczyński J, Beveratos A, Krebs O, Lemaître A, Sagnes I, Bloch J, Voisin P and Senellart P 2010 Ultrabright source of entangled photon pairs *Nature* **466** 217

[22] Hennessy K, Badolato A, Winger M, Gerace D, Atature M, Gulde S, Fălt S, Hu E L and Ǐmamoḡlu A 2007 Quantum nature of a strongly coupled single quantum dot–cavity system *Nature* **445** 896

[23] Nomura M, Kumagai N, Iwamoto S, Ota Y and Arakawa Y 2010 Laser oscillation in a strongly coupled single-quantum-dot–nanocavity system *Nature Phys.* **6** 279

[24] Ota Y, Iwamoto S, Kumagai N and Arakawa Y 2011 Spontaneous two-photon emission from a single quantum dot *Phys. Rev. Lett.* **107** 233602

[25] Laucht A, Villas-Bôas J M, Stobbe S, Hauke N, Hofbauer F, Böhm G, Lodahl P, Amannand M-C, Kaniber M and Finley J J 2010 Mutual coupling of two semiconductor quantum dots via an optical nanocavity *Phys. Rev.* B **82** 075305

IOP Institute of Physics ⦿ DEUTSCHE PHYSIKALISCHE GESELLSCHAFT

[26] Gallardo E *et al* 2010 Optical coupling of two distant InAs/GaAs quantum dots by a photonic-crystal microcavity *Phys. Rev.* B **81** 193301

[27] Schneebeli L, Kira M and Koch S W 2008 Characterization of strong light–matter coupling in semiconductor quantum-dot microcavities via photon-statistics spectroscopy *Phys. Rev. Lett.* **101** 097401

[28] Kasprzak J, Reitzenstein S, Muljarov E A, Kistner C, Schneider C, Strauss M, Höfling S, Forchel A and Langbein W 2010 Up on the Jaynes–Cummings ladder of a quantum-dot/microcavity system *Nature Mater.* **9** 304

[29] Laussy F P, del Valle E, Schrapp M, Laucht A and Finley J J 2012 Climbing the Jaynes–Cummings ladder by photon counting *J. Nanophoton.* **6** 061803

[30] Majumdar A, Bajcsy M and Vuckovic J 2012 Probing the ladder of dressed states and nonclassical light generation in quantum-dot–cavity QED *Phys. Rev.* A **85** 041801

[31] del Valle E, Zippilli S, Laussy F P, Gonzalez-Tudela A, Morigi G and Tejedor C 2010 Two-photon lasing by a single quantum dot in a high-Q microcavity *Phys. Rev.* B **81** 035302

[32] del Valle E, Gonzalez-Tudela A, Cancellieri E, Laussy F P and Tejedor C 2011 Generation of a two-photon state from a quantum dot in a microcavity *New J. Phys.* **13** 113014

[33] del Valle E, Gonzalez-Tudela A and Laussy F P 2012 Generation of a two-photon state from a quantum dot in a microcavity under incoherent and coherent continuous excitation *Proc. SPIE* **8255** 825505

[34] Stace T M, Milburn G J and Barnes C H W 2003 Entangled two-photon source using biexciton emission of an asymmetric quantum dot in a cavity *Phys. Rev.* B **67** 085317

[35] Schumacher S, Förstner J, Zrenner A, Florian M, Gies C, Gartner P and Jahnke F 2012 Cavity-assisted emission of polarization-entangled photons from biexcitons in quantum dots with fine-structure splitting *Opt. Express* **20** 5335

[36] del Valle E, Gonzalez-Tudela A, Laussy F P, Tejedor C and Hartmann M J 2012 Theory of frequency-filtered and time-resolved N-photon correlations *Phys. Rev. Lett.* **109** 183601

[37] Mollow B R 1969 Power spectrum of light scattered by two-level systems *Phys. Rev.* **188** 1969

[38] Gonzalez-Tudela A, Laussy F P, Tejedor C, Hartmann M J and del Valle E 2012 Two-photon spectra of quantum emitters arXiv:1211.5592

[39] Arnoldus H F and Nienhuis G 1984 Photon correlations between the lines in the spectrum of resonance fluorescence *J. Phys. B: At. Mol. Phys.* **17** 963

[40] Knöll L and Weber G 1986 Theory of n-fold time-resolved correlation spectroscopy and its application to resonance fluorescence radiation *J. Phys. B: At. Mol. Phys.* **19** 2817

[41] Cresser J D 1987 Intensity correlations of frequency-filtered light fields *J. Phys. B: At. Mol. Phys.* **20** 4915

[42] Aspect A, Roger G, Reynaud S, Dalibard J and Cohen-Tannoudji C 1980 Time correlations between the two sidebands of the resonance fluorescence triplet *Phys. Rev. Lett.* **45** 617

[43] Schrama C A, Nienhuis G, Dijkerman H A, Steijsiger C and Heideman H G M 1991 Destructive interference between opposite time orders of photon emission *Phys. Rev. Lett.* **67** 2443–5

[44] Centeno Neelen R, Boersma D M, van Exter M P, Nienhuis G and Woerdman J P 1993 Spectral filtering within the Schawlow–Townes linewidth as a diagnostic tool for studying laser phase noise *Opt. Commun.* **100** 289

[45] Moreau E, Robert I, Manin L, Thierry-Mieg V, Gérard J M and Abram I 2001 Quantum cascade of photons in semiconductor quantum dots *Phys. Rev. Lett.* **87** 183601

[46] Press D, Götzinger S, Reitzenstein S, Hofmann C, Löffler A, Kamp M, Forchel A and Yamamoto Y 2007 Photon antibunching from a single quantum dot–microcavity system in the strong coupling regime *Phys. Rev. Lett.* **98** 117402

[47] Kaniber M, Laucht A, Neumann A, Villas-Bôas J M, Bichler M, Amann M-C and Finley J J 2008 Investigation of the nonresonant dot–cavity coupling in two-dimensional photonic crystal nanocavities *Phys. Rev.* B **77** 161303

[48] Sallen G, Tribu A, Aichele T, André R, Besombes L, Bougerol C, Richard M, Tatarenko S, Kheng K and Poizat J-Ph 2010 Subnanosecond spectral diffusion measurement using photon correlation *Nature Photon.* **4** 696

IOP Institute of Physics   **Φ** DEUTSCHE PHYSIKALISCHE GESELLSCHAFT

[49] Ulhaq A, Weiler S, Ulrich S M, Roßbach R, Jetter M and Michler P 2012 Cascaded single-photon emission from the Mollow triplet sidebands of a quantum dot *Nature Photon.* **6** 238

[50] Bel G and Brown F L H 2009 Theory for wavelength-resolved photon emission statistics in single-molecule fluorescence spectroscopy *Phys. Rev. Lett.* **102** 018303

[51] Eberly J H and Wódkiewicz K 1977 The time-dependent physical spectrum of light *J. Opt. Soc. Am.* **67** 1252

[52] Benson O, Santori C, Pelton M and Yamamoto Y 2000 Regulated and entangled photons from a single quantum dot *Phys. Rev. Lett.* **84** 2513

[53] Troiani F, Perea J I and Tejedor C 2006 Analysis of the photon indistinguishability in incoherently excited quantum dots *Phys. Rev.* B **73** 035316

[54] Meirom E A, Lindner N H, Berlatzky Y, Poem E, Akopian N, Avron J E and Gershoni D 2008 Distilling entanglement from random cascades with partial 'which path' ambiguity *Phys. Rev.* A **77** 062310

[55] Pfanner G, Seliger M and Hohenester U 2008 Entangled photon sources based on semiconductor quantum dots: the role of pure dephasing *Phys. Rev.* B **78** 195410

[56] Avron J E, Bisker G, Gershoni D, Lindner N H, Meirom E A and Warburton R J 2008 Entanglement on demand through time reordering *Phys. Rev. Lett.* **100** 120501

[57] Johne R, Gippius N A, Pavlovic G, Solnyshkov D D, Shelykh I A and Malpuech G 2008 Entangled photon pairs produced by a quantum dot strongly coupled to a microcavity *Phys. Rev. Lett.* **100** 240404

[58] Pathak P K and Hughes S 2009 Generation of entangled photon pairs from a single quantum dot embedded in a planar photonic-crystal cavity *Phys. Rev.* B **79** 205416

[59] Carmele A, Milde F, Dachner M-R, Harouni M B, Roknizadeh R, Richter M and Knorr A 2010 Formation dynamics of an entangled photon pair: a temperature-dependent analysis *Phys. Rev.* B **81** 195319

[60] Carmele A and Knorr A 2011 Analytical solution of the quantum-state tomography of the biexciton cascade in semiconductor quantum dots: pure dephasing does not affect entanglement *Phys. Rev.* B **84** 075328

[61] Poddubny A N 2012 Effect of continuous and pulsed pumping on entangled photon pair generation in semiconductor microcavities *Phys. Rev.* B **85** 075311

[62] Scully M O, Englert B-G and Walther H 1991 Quantum optical tests of complementarity *Nature* **351** 111

[63] Chuan W and Yong Z 2009 Quantum secret sharing protocol using modulated doubly entangled photons *Chin. Phys.* **18** 3238

[64] Wang H, Liu S and He J 2009 Thermal entanglement in two-atom cavity QED and the entangled quantum otto engine *Phys. Rev.* E **79** 041113

[65] Trotta R, Zallo E, Ortix C, Atkinson P, Plumhof J D, van den Brink J, Rastelli A and Schmid O G 2012 Universal recovery of the energy-level degeneracy of bright excitons in InGaAs quantum dots without a structure symmetry *Phys. Rev. Lett.* **109** 147401

[66] Wootters W K 1998 Entanglement of formation of an arbitrary state of two qubits *Phys. Rev. Lett.* **80** 2245

[67] Munro W J, James D F V, White A G and Kwiat P G 2001 Maximizing the entanglement of two mixed qubits *Phys. Rev.* A **64** 030302